ISSN 1070-3284, Russian Journal of Coordination Chemistry, 2021, Vol. 47, No. 1, pp. 88–94. © Pleiades Publishing, Ltd., 2021.

Synthesis, Structure and Photophysical Properties of 1,8-Naphthalimidyl-Derived Schiff Base and Its Boron Complex

L. B. Gao*

College of Chemistry and Pharmaceutical Sciences, Qingdao Agriculture University, Qingdao, 266109 P.R. China

**e-mail: lbgao@qau.edu.cn*

Received February 8, 2020; revised March 24, 2020; accepted March 27, 2020

Abstract—A novel Schiff base containing 1,8-naphthalimidyl group (L) and its boron complex $C_{27}H_{29}BN_4O_2F_2$ (**I**) were successfully synthesized and their structures were confirmed by using elemental analysis, UV–Vis, ESI-MS, ^{1}H NMR and ^{13}C NMR spectroscopies. The fluorescence properties of new Schiff base L as well as its boron complex **I** were investigated. X-ray single crystal analysis of boron complex **I** (CIF file CCDC no. 1888435) reveals that the coordination of BF_2 with one of the hydrazone group nitrogens (N(2)) along with the pyridyl nitrogen (N(3)) forms a six-membered ring. The boron atom adopts a tetrahedral geometry and the plane defined by F–B–F atoms is perpendicular to that of the central C(2)N(3) core. One-dimensional chains were formed along the *b* axis through weak π–π interactions and the adjacent molecular are stabilized by C–H···O hydrogen bonds interactions, forming a three-dimensional architecture. Luminescent properties reveal that the emission wavelength is blue-shifted whether in CH_2Cl_2 solution or in crystal state after the ligand was coordinated by BF_2 fragment. The Stokes shift for **I** is about 73 nm, which may have been caused by the intramolecular hydrogen bonds dominated by the oxygen atom and the nitrogen atom and the distortion of the molecular structure.

Keywords: Schiff base, boron complex, crystal structure, fluorescence properties

DOI: 10.1134/S1070328420120039

INTRODUCTION

Boron complexes have attracted considerable attention due to their diverse coordination chemistry and tunable emission wavelengths and high fluorescence quantum yields [1–3]. In particular, boron dipyrromethene (BODIPY) derivatives have played significant roles in many fields such as molecular sensors [4–6], biomolecular probes [7, 8], and in the construction of optoelectronic devices such as organic light emitting devices (OLEDs) [9]. Although boron complexes are strongly emissive in solution, most of them suffer from aggregation induced quenching (ACQ) owing to the self-absorption enhanced by the small Stokes shifts and intermolecular π–π interactions caused by the symmetric and planar structure. To overcome this obstacle, various strategies have been developed such as aggregation-induced emission (AIE) [10, 11] and introduction of bulky groups [12]. Aprahamian and co-workers reported a new family of BF_2-hydrazone complexes which exhibit enhanced emission in the solid state. The high fluorescence quantum yields in the solid state were derived from a balance between planarity and intermolecular π–π interactions [13]. Tian and co-workers developed a series of novel 2,2'-biindenyl based fluorophores based on the AIE strategy and studied their solid-state emission which can be readily tuned by the variation of the substituents on the 2,2'-biindenyl fluorophore [14]. Shen and co-worker prepared a series of arylsilyl-substituted BODIPY dyes. Their solid-state emissions were efficiently improved by the introduction of triphenylsilylphenyl and triphenylsilylphenyl (ethynyl) as bulky groups [15]. Within many reported boron complexes, naphthalene or 1,8-naphthalimide unit as bulky groups were rarely studied [16, 17]. 1,8-Naphthalimide unit as an electron deficient buiding block has many advantages, such as (1) the absorption and emission at long wavelengths, (2) long range intermolecular charge delocalization of the π-electron cloud, and (3) the photophysical properties of the naphthalimide structure governed by the nature of the substituent and the substitution pattern employed at active C-4 and N-atom positions which are easily functionalized. According to the Cambridge Structural Database, there are only several reports on investigations of the structures and photophysical properties of boron complexes containing 1,8-naphthalimide unit. Kubo and coworkers designed and synthesized a 1-hydroxy-2,3,1-benzodiazaborine conjugated with 1,8-naphthalimide [18]. The X-ray diffraction analysis showed that the benzodiazaborine adopted almost a planar π-conjugation. The dihedral angle between benzodiazaborine and naphthalimide unit was 47.3° which caused a large Stokes shift in the fluorescence

spectra. The emission position and the fluorescent quantum yields were affected by the polarity of the solvent. The related solid luminescence of the boron complexe was not investigated.

In this paper, we report the synthesis and characterization of a novel Schiff base (L) containing 1,8-naphthalimidyl group and its boron complex $C_{27}H_{29}BN_4O_2F_2$ (**I**), which are shown in Scheme 1. To get understanding of the effect of BF_2 group, the crystal structure of boron complex (**I**) and their photophysical properties in CH_2Cl_2 and crystalline state are investigated.

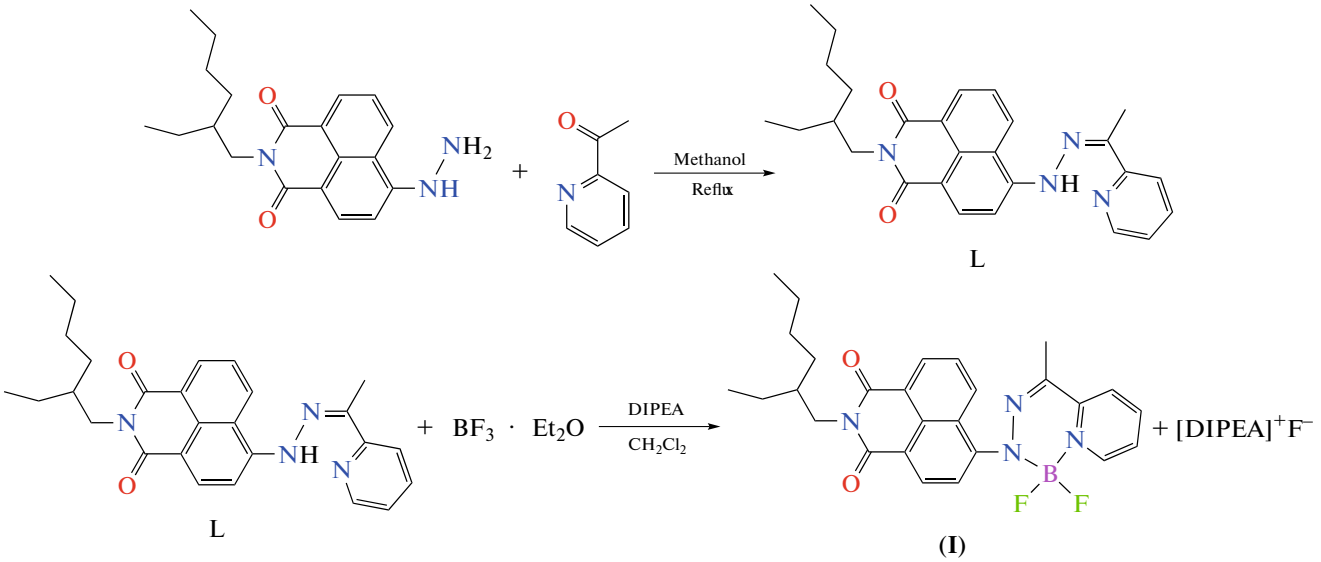

(DIPEA = *N,N*-diisopropylethylamine)

Scheme 1.

EXPERIMENTAL

Materials and measurements. All starting materials were purchased commercially as reagent grade and used as received unless otherwise mentioned. Dichloromethane was distilled over calcium hydride. The solvents used for spectroscopic measurements were of HPLC grade. The corresponding 4-hydrazino-*N*-(2-ethylhexyl)-1,8-naphthalimide was synthesized according to the literature methods [19]. ^{1}H NMR and ^{13}C NMR spectra were recorded on a Bruker DRX-600 spectrometer. Electrospray ionization mass spectra (ESI-MS) were recorded on a Bruker maxis UHR-TOF mass spectrometer. The ultraviolet-visible (UV–Vis) spectra and photoluminescence (PL) spectra were measured on a Lambda 25 spectrophotometer and HORIBA JOBIN YVON FluoroMax-4 spectrophotometer, respectively.

Synthesis of 1-(2-pyridyl)ethan-1-one-*N*-(2-ethylhexyl)-1,8-naphthalimide hydrazone (L). To a solution of 4-hydrazino-*N*-(2-ethylhexyl)-1,8-naphthalimide (0.177 g, 0.4 mmol) in methanol (25 mL) was added 2-acetylpyridine (0.048 g, 0.4 mmol) under Ar atmosphere. The resulting mixture was heated under reflux for 12 h. After the reaction, the mixture was slowly cooled to the room temperature. Crystals formed upon standing were filtered off, washed with methanol and dried to obtain compound L as a brown solid. The yield was 0.120 g (68%).

For $C_{27}H_{30}N_4O_2$			
Anal. calcd., %	C, 73.28	H, 6.83	N, 12.66
Found, %	C, 73.21	H, 6.79	N, 12.60

^{1}H NMR ($CDCl_3$; 600 MHz; δ, ppm): 15.56 (s., 1H, N–H), 8.83 (s., 1H, Py), 8.57 (d., J = 6.9 Hz, 1H, arom. $C_{10}H_5$), 8.52 (d., J = 8.3 Hz, 1H, arom. $C_{10}H_5$), 8.25 (d., J = 7.9 Hz, 1H, Py), 7.93 (t., J = 7.4 Hz, 1H, arom. $C_{10}H_5$), 7.84 (d., J = 8.3 Hz, 1H, arom. $C_{10}H_5$), 7.67 (t., J = 7.4 Hz,1H, Py), 7.61 (d., J = 7.9 Hz, 1H, arom. $C_{10}H_5$), 7.41 (t., J = 5.2 Hz, 1H, Py), 4.14–4.05 (m, 2H, N–CH_2, aliphatic), 2.52 (s., 3H, CH_3), 1.96 (m., 1H, CH, aliphatic), 1.40–1.31 (m., 8H, CH_2, aliphatic), 0.93 (t., J = 7.2 Hz, 3H, CH_3, aliphatic), 0.88 (t., J = 6.7 Hz, 3H, CH_3, aliphatic); ^{13}C NMR ($CDCl_3$; 150 MHz; δ, ppm): 165.1, 164.5, 153.7, 147.2, 146.2, 137.9, 137.7, 134.1, 130.9, 129.8, 126.7, 125.1, 123.7, 123.4, 123.1, 119.5, 112.6, 106.9, 43.9, 38.0, 30.8, 28.8, 24.1, 23.1, 22.3, 14.1, 10.7. ESI-MS *m/z*: 443.3 ($[M+H]^+$).

Synthesis of boron complex I. To a solution of hydrazone L (0.100 g, 0.23 mmol) in dry methylene chloride at room temperature was added DIPEA

(7 equiv, 0.27 mL, 1.61 mmol). After 2 h, boron trifluoride diethyl ether complex (10 equiv, 2.9 mL, 23 mmol) was added dropwise. The reaction mixture was stirred at room temperature overnight. The reaction mixture was quenched with water and extracted by methylene chloride. The organic layer was washed three times with 10 mL water and dried over magnesium sulfate. After solvent concentration, the crude product was subjected to silica gel column chromatography (hexane/ethyl acetate 5 : 1) to give boron complex **I** as a bright orange solid. The yield was (0.032 g, 28%).

For $C_{27}H_{29}BN_4O_2F_2$			
Anal. calcd., %	C, 66.13	H, 5.96	N, 11.43
Found, %	C, 66.11	H, 5.93	N, 11.40

^{1}H NMR ($CDCl_3$; 600 MHz; δ, ppm): 8.80 (d., J = 5.8 Hz, 1H, Py), 8.62 (d., J = 7.9 Hz, 1H, arom. $C_{10}H_5$), 8.59 (d., J = 7.2 Hz, 1H, arom. $C_{10}H_5$), 8.52 (d., J = 8.6 Hz, 1H, Py), 8.28 (t., J = 7.4 Hz,1H, arom. $C_{10}H_5$), 7.83 (d., J = 8.0 Hz, 1H, arom. $C_{10}H_5$), 7.81 (d., J = 8.4 Hz, 1H, arom. $C_{10}H_5$), 7.72 (t., J = 7.2 Hz, 1H, Py), 7.66 (t., J = 7.3 Hz, 1H, Py), 4.18–4.10 (m, 2H, N-CH_2, aliphatic), 2.57 (s., CH_3), 1.97 (m., 1H, CH, aliphatic), 1.40–1.30 (m., 8H, CH_2, aliphatic), 0.94 (t., J = 7.5 Hz, 3H, CH_3, aliphatic), 0.88 (t., J = 7.1 Hz, 3H, CH_3, aliphatic); ^{13}C NMR ($CDCl_3$; 150 MHz; δ, ppm): 164.9, 164.4, 148.4, 142.4, 141.4, 139.9, 131.9, 131.2, 129.9, 127.9, 125.9, 124.0, 122.7, 122.6, 121.5, 119.5, 44.1, 37.9, 30.8, 29.7, 28.8, 24.1, 23.1, 22.7, 19.1, 14.1, 10.7. ESI-MS m/z: 491.5 ($[M+H]^+$).

X-ray structure determination. The selected crystal was mounted on a Bruker D8 Quest ECO diffractometer at room temperature. The collected data were reduced by using the program SAINT [20]. The structure was solved by direct methods and refined by full-matrix least-squares using SHELXL-97 program [21, 22]. The non-hydrogen atoms were located in successive different Fourier syntheses and refined with anisotropic thermal parameters. The hydrogen atoms of the ligands were generated theoretically onto the specific atoms and refined with isotropic thermal parameters. The summary of the key crystallographic information of compound **I** is given in Table 1. The selected bond lengths and angles are listed in Table 2.

Supplementary material for **I** has been deposited with the Cambridge Crystallographic Data Centre (CCDC no. 1888435; deposit@ccdc.cam.ac.uk or http://www.ccdc.cam.ac.uk).

RESULTS AND DISCUSSION

The synthetic procedure of **I** is depicted in Scheme 1. Schiff base L was prepared according to the condensation method of 4-hydrazino-*N*-(2-ethylhexyl)-1,8-naphthalimide with 2-acetylpyridine in methanol under reflux conditions for 12 h. After workup, the Schiff base ligand L was treated with boron trifluoride diethyl ether in the present of *N*,*N*-diisopropylethylamine to obtain the final boron product **I**. The L ligand and complex **I** are brown and bright orange solid, respectively. Both ligand L and complex **I** are fully characterized by NMR, mass spectrum, and microanalysis. In the ^{1}H NMR spectra, the proton on the nitrogen atom of secondary amine observed at 15.56 ppm for ligand L was disappeared when it was coordinated with BF_2 fragment. All proton signals can be easily assigned to each the corresponding hydrogen, and the integration is well consistent with the hydrogen numbers. Moreover, the proposed structures of L and **I** were confirmed by $[M+H]^+$ ion peaks in ESI-MS and single-crystal X-ray analysis of **I**.

Single crystals of **I** suitable for X-ray analysis were obtained by slow evaporation of dichloromethane solutions. The analysis of **I** shows that the crystal belongs to the monoclinic system and crystallizes in space group $P2_1/c$ with four molecules in the unit cell. Figure 1 shows the molecular structure and hydrogen bonding interactions. Bond distances and angles are unexceptional. The hexyl side chains in the molecule adopt a disordered conformations. The boron atom is coordinated in a tetrahedral geometry by two nitrogen and two fluorine atoms and the plane defined by F–B–F atoms is almost perpendicular to that of the central C(2)N(3) core. The indacene plane is highly planar with average root-mean-square deviation of 0.0742 Å. The dihedral angles between the indacene plane and the pyridinyl ring is 4.31(0.20)°, which implies partial electronic coupling between the indacene plane and pyridinyl ring. The naphthalimide unit is tilted by 40.89(0.13)° with respect to the indacene plane (Fig. 1a), which may have caused the relatively large Stokes shifts in the fluorescence spectra. The B–N(2) and B–N(3) bond lengths are 1.517(5) and 1.566(5) Å, which are compared to the 1.44 Å bond length of borazine [23]. The bulky naphthalimide unit and BF_2 fragment lead to enhanced distortion of the molecular structure and inhibit π–π stacking. As is shown in Fig. 1b, the distance between the nearest neighbor planes is 3.338(14) Å. It is interesting to explore the architecture of the boron complex **I**, two hydrogen bonds in C(14)–H(14*A*)···O(1) and C(1)–H(1*B*)···O(2) are the predominant intermolecular interactions and their bond lengths are 3.323(5) and 3.151(5) Å, respectively (Table 3). One-dimensional chains were formed along the *b* axis through weak π–π interactions and the adjacent molecular are stabilized by C–H···O hydrogen bonds interactions, forming a three-dimensional architecture.

The spectral data of UV–Vis absorption and emission spectra for L and **I** were measured in CH_2Cl_2 solutionin and are displayed in Fig. 2a. The corre-

Table 1. Crystallographic data and structure refinement for complex **I**

Parameter	Value
Formula weight	491.36
T, K	296(2)
Wavelength, Å	0.71073
Crystal system; space group	Monoclinic; $P2_1/c$
a, Å	5.0490(6)
b, Å	15.8409(17)
c, Å	30.739(3)
β, deg	92.315(3)
Volume, Å^3	2456.5(5)
Z	4
ρ_{calcd}, mg/m^3	1.329
μ, mm^{-1}	0.095
F(000)	1036
Crystal size, mm	0.330 × 0.182 × 0.073
Limiting indices	$-6 \le h \le 6$, $-18 \le k \le 18$, $-36 \le 1 \le 35$
Reflections collected/unique	31867/4280
R_{int}	0.1029
Completeness to θ = 24.99, %	99.7
Data/restraints/parameters	4280/10/335
Goodness-of-fit on F^2	1.025
R_1, wR_2 ($I > 2\sigma(I)$)	0.0680, 0.1475
R_1, wR_2 (all data)	0.1500, 0.1862
Largest diff. peak and hole, e Å^{-3}	0.333 and −0.292

sponding optical parameters are summarized in Table 4. As shown in Table 4, the absorption bands of L and **I** at about 350 nm are assigned to π−π* transition of naphthalimide moieties. The lowest energy absorption maxima at 435 nm for **I** and 468 nm for L were attributed to S_0-S_1 transition. The absorption peaks for **I** are a little blue-shifted compared with those of L, because of the lower-energy absorption of **I** is ascribed to the distortion of the molecular structure enhancing the transition energy. The same trend was observed in the emission spectra of L and **I**.

Luminescent properties of ligands L and **I** were investigated in CH_2Cl_2 solution and in crystalline state at room temperature. As shown in Fig. 2b, the fluorescent spectra display emissions at 508 and 520 nm for **I** and L in CH_2Cl_2, respectively, which can be assigned to intraligand transition. Compared with L, the emission wavelength of **I** is blue-shifted by about 10 nm. The Stokes shift for **I** is about 73 nm which may have been caused by the intramolecular hydrogen bonds dominated by the oxygen atom and the nitrogen atom and the distortion of the molecular structure. As shown in Fig. 3, PL microscopy images revealed that both complexes were all in rodlike microstructures. The emission behavior of crystalline L and **I** were tested. The crystals of L showed red fluorescence with

Table 2. Selected bond lengths (Å) and bond angles (deg) for **I**

Bond		*d*, Å	
B–F(1)	1.360(5)	C(6)–N(1)	1.292(5)
B–F(2)	1.383(5)	C(8)–N(2)	1.409(4)
B–N(2)	1.517(5)	N(4)–C(18)	1.399(5)
B–N(3)	1.566(5)	N(1)–N(2)	1.351(4)
C(1)–N(3)	1.343(4)	N(4)–C(19)	1.396(5)
C(1)–C(2)	1.368(5)	N(4)–C(20)	1.476(4)
C(5)–N(3)	1.354(4)	O(1)–C(18)	1.222(4)
Angle		ω, deg	
F(1)BF(2)	109.7(3)	C(6)N(1)N(2)	121.1(3)
F(1)BN(2)	111.6(3)	N(1)N(2)C(8)	115.7(3)
F(1)BN(2)	112.5(3)	N(1)N(2)B	123.3(3)
F(1)BN(3)	109.2(3)	C(8)N(2)B	120.5(3)
F(2)BN(3)	105.5(3)	C(1)N(3)C(5)	119.8(3)
N(2)BN(3)	108.0(3)	C(1)N(3)B	117.7(3)
N(3)(1)C(2)	122.4(4)	C(5)N(3)B	122.3(3)

Table 3. Geometric parameters of hydrogen bond for **I**

D–H···A	Distance, Å			D–H···A, deg
	D–H	H···A	D···A	
C(1)–H(1B)···O(2)	0.93	2.5900	3.151(5)	120
C(14)–H(14A)···O(1)	0.93	2.5500	3.323(5)	141
C(20)–H(20A)···O(2)	0.97	2.3400	2.724(5)	103
C(16)–H(16)A···N(1)	0.93	2.3200	2.884(5)	119
C(9)–H(9A)···F(2)	0.93	2.3500	3.031(4)	130

λ_{max} at 610 nm and low Φ_F of 0.11 (Φ_F is fluorescence quantum yield). When the ligand was coordinated by BF_2 fragment, however, the crystals of **I** exhibited green emission color at 515 nm with higher Φ_F of 0.19. The emission peak of L exhibited a red-shift emission about 90 nm from solution to crystal, which was mainly due to its distorted configuration in solution, and unique crystal packing mode in solid. However, the emission peak of **I** in solution (508 nm) was close to the solid state emission peak (515 nm), which might be that the packing mode has very limited effect on their solid emission peak.

Table 4. Photophysical data for L and **I**

Compound	λ_{abs}, nm	λ_{em}, nm	Φ_F
L (CH_2Cl_2)	324, 468	520	0.24
(crystal)		610	0.11*
I (CH_2Cl_2)	352, 435	508	0.32
(crystal)		515	0.19*

* Determined as an absolute fluorescence quantum yield with an integration sphere in crystal state.

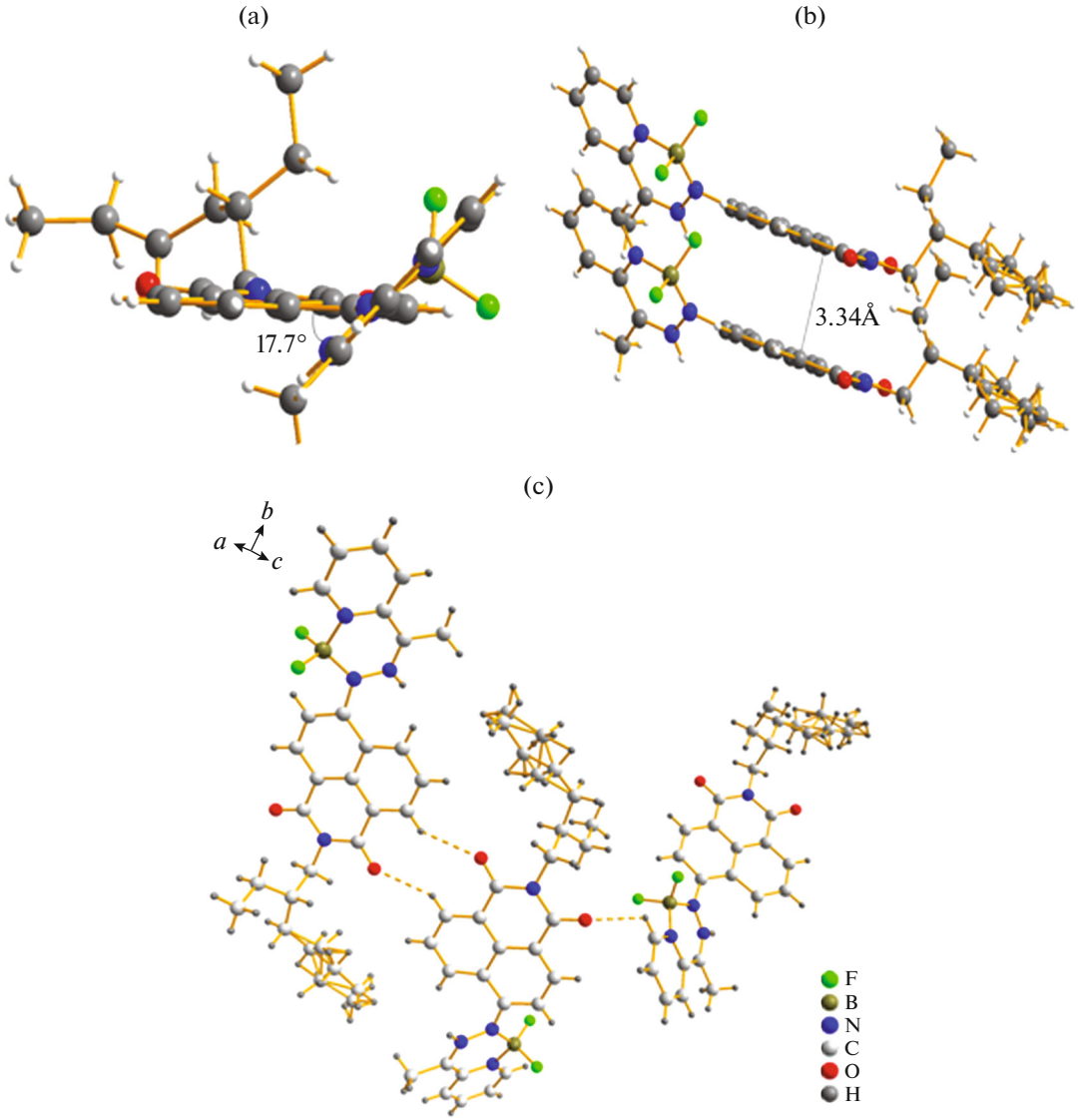

Fig. 1. X-ray crystal structure of **I**: the front view (a), packing structure (b) and intermolecular hydrogen bonding interactions (c).

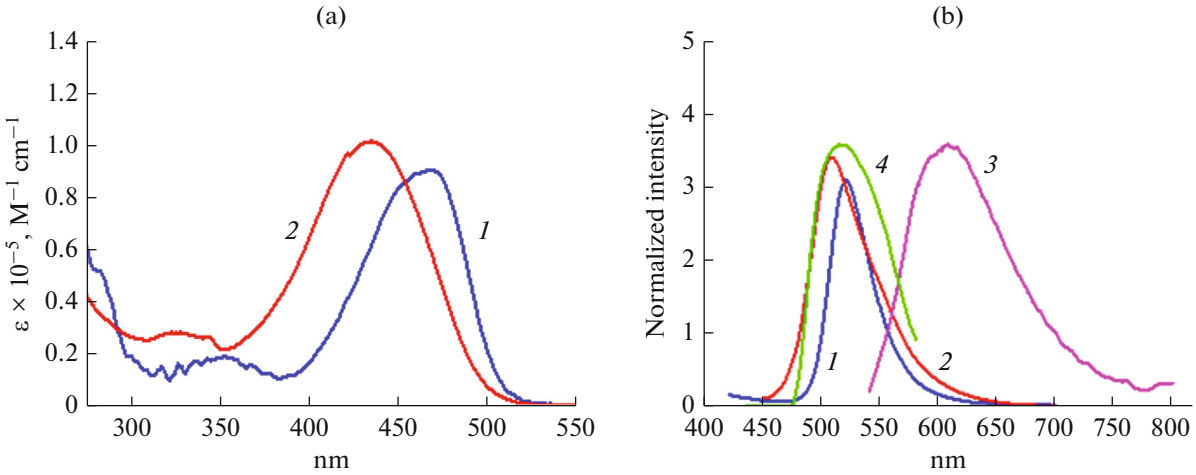

Fig. 2. UV–Vis absorption spectra for L (*1*) and **I** (*2*) in CH_2Cl_2 (a); PL emission spectra of L (*1*) and **I** (*2*) in CH_2Cl_2 and in the crystalline state (*3, 4*, respectively (b)).

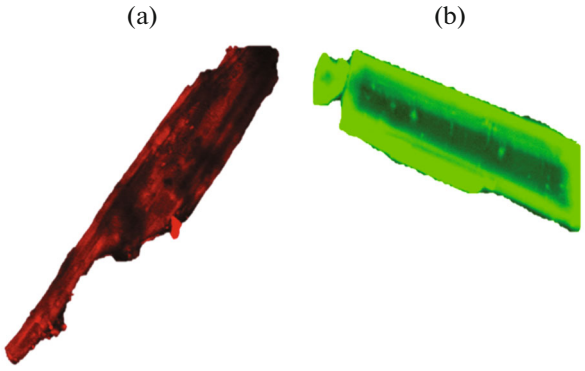

Fig. 3. Fluorescence images of L (a) and **I** (b).

FUNDING

We appreciate the financial support from Shandong Provincial Natural Science Foundation (ZR2018LB015); the Scientific Research Foundation of Qingdao Agricultural University.

CONFLICT OF INTEREST

The authors declare that they have no conflicts of interest.

REFERENCES

1. Nelyubin, A.V., Klyukin, I.N., Zhdano, A.P., et al., *Russ. J. Inorg. Chem.*, 2019, p. 1499. https://doi.org/10.1134/S003602361912012X
2. Avdeeva, V.V., Vologzhanin, A.V., Malinin, E.A., et al., *Russ. J. Coord. Chem.*, 2019, vol. 45, p. 295. https://doi.org/10.1134/S1070328419040018
3. Sivaev, I.B., *Russ. J. Inorg. Chem.*, 2019, vol. 64, p. 955. https://doi.org/10.1134/S003602361908014X
4. Burn, P.L., Lo, S.-C., and Samuel, I.D.W., *Adv. Mater.*, 2007, vol. 19, p. 1675.
5. Saragi, T.P.I., Spehr, T., Siebert, A., et al., *Chem. Rev.*, 2007, vol. 107, p. 1011.
6. Grimsdale, A.C., Chan, K.L., Martin, R.E., et al., *Chem. Rev.*, 2009, vol. 109, p. 897.
7. Hatakeyama, T., Hashimoto, S., Seki, S., and Nakamura, M., *J. Am. Chem. Soc.*, 2011, vol. 133, p. 18614.
8. van de Wouw, H.L., Lee, J.Y., Siegler, M.A., and Klausen, R.S., *Org. Biomol. Chem.*, 2016, vol. 14, p. 3256.
9. Shimizu, M. and Hiyama, T., *Chem. Asian J.*, 2010, vol. 5, p. 1516.
10. Hong, Y., Lam, J.W.Y., and Tang, B.Z., *Chem. Commun.*, 2009, p. 4332.
11. Hong, Y., Lam, J.W.Y., and Tang, B.Z., *Chem. Soc. Rev.*, 2011, vol. 40, p. 5361.
12. Zhang, D., Wen, Y., Xiao, Y., et al., *Chem. Commun.*, 2008, p. 4777.
13. Yang, Y., Hughes, R.P., and Aprahamian, I., *J. Am. Chem. Soc.*, 2012, vol. 134, p. 15221.
14. Zhang, Z., Chen, C., Chen, Y., et al., *Angew. Chem. Int. Ed.*, 2018, vol. 57, p. 9880.
15. Liu, H., Lu, H., Zhou, Z., et al., *Chem. Commun.*, 2015, vol. 51, p. 1713.
16. Zhu, W.J., Qin, Z.J., Bai, Y., and Dang, D.B., *Russ. J. Coord. Chem.*, 2018, vol. 44, p. 425. https://doi.org/10.1134/S1070328418070096
17. Sergienko, V.S., Koksharova, T.V., Surazhskaya, M.D., and Skakun, T.S., *Russ. J. Inorg. Chem.*, 2018, vol. 63, p. 1171. https://doi.org/10.1134/S0036023618090176
18. Satta, Y., Nishiyabu, R., James, T.D., and Kubo, Y., *Tetrahedron*, 2017, vol. 73, p. 2053.
19. Gudeika, D., Lygaitis, R., Mimait, V., et al., *Dyes Pigments*, 2011, vol. 91, p. 13.
20. SAINT, Version 6.45, Bruker Analytical X-ray Systems Inc., 2003.
21. Sheldrick, G.M., *SHELXS-97, Program for Crystal Structure Solution and Refinement*, Göttingen: Univ. of Göttingen, 1997.
22. Sheldrick, G.M., *SHELXL, Crystal Structure Refinement Program*, Göttingen: Univ. of Göttingen, 2013.
23. Satta, Y., Nishiyabu, R., James, T.D., and Kubo, Y., *Tetrahedron*, 2017, vol. 73, p. 2053.